Light-Induced Temperature Jump Causes Power-Dependent Ultrafast Kinetics of Electrons Generated in Multiphoton Ionization of Liquid Water[†]

Robert A. Crowell,*,[‡] Rui Lian,[‡] Ilya A. Shkrob,[‡] Jun Qian,[‡,§] Dmitri A. Oulianov,[‡] and Stanislas Pommeret[‡,⊥]

Chemistry Division, Argonne National Laboratory, 9700 South Cass Avenue, Argonne, Illinois 60439, and CEA/Saclay, DSM/DRECAM/SCM/URA 331 CNRS 91191 Gif-Sur-Yvette Cedex, France

Received: May 4, 2004; In Final Form: July 1, 2004

Picosecond geminate recombination kinetics for electrons generated by multiphoton ionization of liquid water become power dependent when the irradiance of the excitation light is greater than $0.3-0.5$ TW/cm^2 (the terawatt regime). To elucidate the mechanism of this power dependence, tri- 400 nm photon ionization of water has been studied using pump–probe laser spectroscopy on the pico- and femtosecond time scales. We suggest that the observed kinetic transformations are caused by a rapid temperature jump in the sample. Such a jump is inherent to multiphoton ionization in the terawatt regime, when the absorption of the pump light along the optical path becomes very nonuniform. The heating of water is substantial (tens of °C) because the 3-photon quantum yield of the ionization is relatively low, ca. 0.42, and a large fraction of the excitation energy is released into the solvent bulk as heat. Evidence of the temperature jump is the observation of a red shift in the absorption spectrum of (thermalized) electron and by characteristic "flattening" of the thermalization dynamics in the near-IR The temperature jump in the terawatt regime might be ubiquitous in multiphoton ionization of molecular liquids. The implications of these observations for femtosecond pulse radiolysis of water are discussed.

1. Introduction

Multiphoton ionization of liquid water exhibits two distinct energetic regimes that are determined by the total excitation energy: When this total energy is below a certain threshold value (ca. 9.5 eV), the spatial distribution of the ejected photoelectrons (e_{aq}^-) around their parent holes is narrow (ca. 1 nm in width) and the geminate recombination of these electrons is relatively fast. Above this threshold energy, the distribution increases to $2-3$ nm (ca. 12.4 eV) and the geminate recombination kinetics becomes relatively slow.[1-3] It is believed that the photoelectron ejected in the high-energy ionization process is promoted directly into the conduction band of the liquid, whereas in the low-energy photoionization, an autoionization process occurs, because the energy is insufficient to access this band directly.[1,3] This process should involve a proton transfer in concert with the loss of the electron; the latter is sometimes regarded as an electron transfer to a "pre-existing trap" in the bulk water.[4-6] The width of the initial electron distribution is then defined by the availability of suitable electron traps.[5,6] Several models for this low-energy photoprocess have been suggested (see refs 1 and 3 for more detail); the important point is that in all of these models, such a photoprocess is viewed entirely differently from the high-energy ionization.

Interestingly, the transformation of a narrow electron distribution (that manifests itself through rapid geminate kinetics and low survival probability for the electron) into a broad electron distribution (that manifests itself through slow geminate kinetics and greater survival probability) can be brought about simply by changing the irradiance of the pump light.[1,7-9] Such changes have been observed by several ultrafast spectroscopy groups, including this laboratory. In particular, Crowell and Bartels[1,2] demonstrated that rapid geminate kinetics of hydrated electrons observed in three 400 nm photon ionization of water becomes slower and the fraction of escaped electrons increases when the irradiance of the 400 nm light is in the terawatt range (1 TW/cm$^2 = 10^{16}$ W/m^2). The same trend was observed in the similar terawatt regime by Schwartz et al.[7] and Eisenthal et al.[8] What causes such a dramatic transformation?

Crowell and Bartels suggested that this changeover is caused by the absorption of one or more 400 nm photons by a light-absorbing species generated within the duration of the short excitation pulse (which, in their experiments, was $4-5$ ps fwhm).[1,2] In the following, this mechanism (which may be regarded as the condensed-phase analogue of the above threshold ionization in the gas phase) is referred to as the "3+1" mechanism. The suggestion was made that the species in question is a prethermalized or thermalized (solvated) electron generated in the course of photoionization. Subsequent studies by Barbara and co-workers[10] seemed to support such a scenario: it was shown that one 400 nm photon excitation of fully thermalized, hydrated electron promotes it into the conduction band of the solvent where it thermalizes and localizes after migrating >1 nm away from the hole. Consequently, the geminate recombination is suppressed and the decay of the electron is slowed. This photoprocess is very efficient: the quantum yield of the suppression is near unity. Thus, one of

* To whom correspondence should be addressed. Phone: 630-252-8089. Fax: 630-2524993. E-mail: rob_crowell@anl.gov.
‡ Argonne National Laboratory.
§ Present address: Experimental Facility Division, Advanced Photon Source, Argonne National Laboratory, 9700 South Cass Avenue, Argonne IL 60439. Phone: 630-252-5874. Fax: 630-2529303. E-mail: jqian@aps.anl.gov.
⊥ CEA/Saclay.

the possible mechanisms for the "3+1" photoprocess is the absorption within the duration of the ionizing pulse of a 400 nm photon by the electrons generated in the photoionization process; the electron gains sufficient energy to penetrate deeply into the conduction band of the solvent, reaching the same extended states that are accessed in the course of high-energy water ionization. This "3+1" mechanism naturally explains why the resulting electron distribution is broad.

While such a mechanism seems plausible for picosecond photoionization of water, it is less clear how such a mechanism can account for the changeover in the kinetic behavior observed for shorter, femtosecond pulses. The thermalization of the electron takes a relatively long time (up to 2 ps), whereas the prethermalized electron is a poor light absorber in the blue. In fact, the spectral manifestation of the thermalization/solvation process is a rapid blue shift of the absorption band of the electron initially centered in the near-IR to the visible;[11-15] the initial absorbance of prethermalized electron at 400 nm is negligible.[11,13,14] Even fully thermalized, hydrated electron has relatively low absorptivity at 400 nm (the molar absorptivity is ca. 2600 $M^{-1} cm^{-1}$).[16] Since the photoexcitation of the electron competes with that of the solvent itself, and absorption of 400 nm light by water is very efficient in the terawatt regime, it seems unlikely that a large fraction of photoelectrons can be excited within the duration of a short excitation pulse. The estimates given in the Appendix (see the Supporting Information), using the photophysical parameters determined in section 3.1 of the present work, confirm these suspicions: even in the most favorable scenario, too few electrons would be photoexcited by 400 nm photons, and the observed transition from one kinetic regime to another could not occur. Thus, the only way to explain the observed kinetics changeover by using the "3+1" mechanism is to postulate that some other species, perhaps a short-lived excited state of water, absorbs the extra 400 nm photon. However, this explanation is presently not supported by our data since no light-absorbing state with the postulated properties has been observed on the subpicosecond time scale (section 3.2). Either this 400 nm light-absorbing species has an extremely short lifetime (and then it cannot absorb a sufficiently large number of 400 nm photons to make the "3+1" mechanism efficient) or such a species (e.g., the excited state) does not exist. In the latter case, it becomes unclear what species is responsible for the "3+1" photoexcitation.

In this article, the terawatt regime of 400 nm photoionization of water is reinvestigated on the femto- and picosecond time scales. We argue that the changeover in the kinetic profiles observed in the terawatt regime is caused by a rapid temperature jump, which is inherent to multiphoton ionization in the terawatt regime. The heating of water is substantial (tens of degrees Centigrade) because the 3-photon quantum yield of the ionization is relatively low, ca. 0.42, and a large fraction of the excitation energy is released into the solvent bulk as heat. In this terawatt regime, the absorption of light is extremely nonuniform (for excitation light irradiance >1 TW/cm^2, most of the 400 nm photons are absorbed in a 10 μm thick layer near the surface; see section 3.1), and the local density of the ionization and heat-release events is very high. Above a certain critical concentration (achieved at ca. 1 TW/cm^2) the released heat rapidly (<5 ps) reaches the geminate pair, and the geminate recombination thereby occurs in hot water. Evidence of the temperature jump is the observation of a red shift in the spectrum of (thermalized) electron and by characteristic "flattening" of the thermalization dynamics in the near-IR. The latter effect has also been observed in two 266 nm photon ionization of

water in the terawatt regime.[9,17] For this 266 nm ionization, the 2-photon quantum yield is also relatively low, ca. 0.52.[17a] It is possible that the temperature jump is a general feature of multiphoton ionization of molecular liquids in the terawatt regime.

To save space, the Appendix and Figures 1S to 8S are given in the Supporting Information.

2. Experimental Section

2.1. Laser Spectroscopy. Transient absorbance (TA) measurements reported below were obtained with use of a 1 kHz Ti:sapphire setup, the details of which are given in ref 18a. A diode-pumped Nd:YVO laser was used to pump a Kerr lens mode-locked Ti:sapphire laser operating at 80 MHz (Spectra Physics Tsunami). The 45 fs fwhm pulses from the oscillator were stretched to 80 ps in a single grating stretcher. Single pulses were then selected at 1 kHz with a Pockels cell. The 2 nJ pulses were amplified to 4 mJ in a home-built two-stage multipass Ti:sapphire amplifier. The amplified pulses were passed through a grating compressor that yielded Gaussian probe pulses of 60 fs fwhm and 3 mJ centered at 800 nm. The pulse-to-pulse stability was typically 3%.

The amplified beam was split into two parts. One beam was used to generate the probe pulses while the other was used to generate the 400 nm (second harmonic) pump pulses by frequency doubling in a thin BBO crystal. The pulse energy I_p of 400 nm light was determined with a calibrated thermopile meter (Ophir Optronics model 2A-SH). The probe pulse was derived from the same Ti:sapphire laser beam and delayed in time as much as 500 ps, using a 3-pass 25 mm delay line. For kinetic measurements, 150–200 points acquired on a quasi-logarithmic grid were typically used. If not stated otherwise, the probe pulse was 800 nm. To obtain probe light of wavelength λ other than 800 nm, a white light supercontinuum was generated by focusing the 800 nm light on a 1 mm thick sapphire disk; the probe light was selected using 10 nm fwhm interference filters.

The pump and probe beams were perpendicularly polarized, focused to round spots, and overlapped in the sample at 5°. The spot sizes were determined by scanning the beam with a 10 μm pinhole or by imaging on a CCD array. The maximum fluence of the 400 nm photons was 0.4 J/cm^2. At the high end of this pulse energy range, dielectric breakdown of water was observed. The dielectric breakdown is defined as the formation of an electron–ion plasma that is produced by high 400 nm irradiance. The onset of dielectric breakdown is readily observed by the abrupt onset of scattering of the probe laser beam.[18b] At very high irradiance levels (around 10 TW/cm^2) complete disintegration (steaming, sparking, etc.) of the water jet was observed.

Fast Si photodiodes were used to measure the transmitted and the reference probe and pump light for every laser shot. Testing these photodiodes against the thermopile detector as a function of 400 nm light irradiance showed perfect linearity of the photoresponse over the entire power range. The photodiode signals were amplified and sampled with use of home-built electronics and a 16-bit A/D converter. A mechanical chopper locked at 50% repetition rate of the laser was used to block the pump pulses on alternative shots. The standard deviation for a pump–probe measurement was typically 10 μOD, and the "noise" was dominated by the variation of the pump intensity and flow instabilities in the liquid jet.

In some kinetic measurements, the radius of the pump beam was 2–3 times smaller than the radius of the probe beam

(usually, the pump beam envelops the probe beam at the sample). This "reverse" geometry was used to reduce the sensitivity of the TA signal to imperfections in the 400 nm beam and to minimize the long-term walk-off of the two beams relative to each other as the delay stage is moved. Naturally, the TA signal obtained with the "reverse" beam geometry is much smaller than that obtained with the "normal" beam geometry (pump beam enveloping the probe beam at the sample), and its power dependence is different.

The transmission of 400 nm light T_p, the peak pump irradiance J_p (see eq 1 below) and photoinduced absorbance ΔOD_λ at the probe wavelength λ were determined from these measurements. To obtain the power dependencies, 20−50 series of $(1-5) \times 10^3$ pulses were averaged; the vertical and horizontal bars given in the plots correspond to 95% confidence limits using Pearson analysis. The pump power was continually monitored, and shots in which the absolute deviation of the pulse energy I_p exceeded 1−3% of the mean value were rejected; the same protocol was used to obtain the TA kinetics. The typical rejection rate was 10−50%, depending on the pump power.

It is important to emphasize that white light continuum generation in the water jet was not observed throughout the explored power range (<2 TW/cm^2). We also did not observe (in the specified power range) self-focusing or self-defocusing of the transmitted 400 and 800 nm beams emerging from the jet as their images were telescoped on a screen. These nonlinear effects were too small to substantially change the beam focusing across the thin (70 μm) water jet.

The pulse widths of the pump and probe pulses were determined by harmonic generation in a thin BBO crystal. Alternatively, the rise time of the TA signal from free photo-carriers generated by 400 nm light in a 1.4 μm thick film of amorphous Si:H alloy (8 atom % H) was determined.[19]

2.2. Materials and the Flow System. The experiments were carried out with a homemade high-speed (10 m/s) jet with a stainless steel 90 μm nozzle. In some experiments, a better-quality jet with a 70 μm sapphire nozzle (V. Kyburz AG) was used. To obtain the kinetics in the low-irradiance limit, the kinetic measurements were carried out with (i) a homemade 560 μm thick high-speed jet or (ii) a 5 mm optical path cell with suprasil windows (in the latter case, the pump beam was focused in the center of the cell to avoid damage to the windows). Pure He- or N$_2$-saturated water with dc conductivity <2 nS/cm was circulated by a gear pump in an all 316 stainless steel and Teflon flow system. The experiments above the room temperature were carried out as explained in ref 18a.

3. Results and Discussion

3.1. Power Dependence of Pump Transmission and Product Yield. We first consider an idealized photosystem in which the absorbance of the pump light by the photoproduct(s) is negligible (see ref 17a for the derivation of equations). A more complex situation in which the photoproduct (e.g., the electron) also absorbs the pump light is considered in the Appendix (see the Supporting Information). Let $I(z,r;t)$ be the time-dependent light intensity

$$I(z,r;t) = J_p \exp(-r^2/\rho_p^2 - t^2/\tau_p^2) \tag{1}$$

of the axially symmetric, plane-wave Gaussian laser pulse propagating in the direction z through the medium with n-photon absorption coefficient β_n (here $z = 0$ corresponds to the incidence at the sample). In eq 1, ρ_p and τ_p are the $1/e$ beam radius and pulse width of the Gaussian pulse, respectively, and

J_p is the (peak) pump irradiance (so that the pulse energy I_p is given by $I_p = \pi^{3/2}J_p\rho_p^2\tau_p$). Note that the radius ρ_p defined by eq 1 is $\sqrt{2}$ times smaller than the $1/e$ radius for the electric field amplitude. The absorption of the pump light by the sample is given by the equation

$$\partial I(z,r;t)/\partial z = -\beta_n I(z,r;t)^n \tag{2}$$

and the formation rate of the product (i.e., the electron) generated by simultaneous absorption of n photons with a quantum yield of ϕ_n is given by

$$\frac{\partial c(z,r;t)}{\partial t} = -\frac{\phi_n}{n}\frac{\partial I(z,r;t)}{\partial z} \tag{3}$$

where $c(r,z;t)$ is the concentration of the photoproduct. We will assume that this photoproduct does not absorb the pump light during the laser excitation of water and does not decay in the time interval before detection. From eq 3 we obtain that the optical density of the photoproduct by the end of the photo-excitation pulse is given by

$$\beta_{pr} \int_0^L dz\, c(z,r;t=+\infty) = \phi_n\beta_{pr}/n \int_{-\infty}^{+\infty} dt\, [I(0,r;t) - I(L,r;t)] \tag{4}$$

where L is the sample thickness and β_{pr} is the absorption coefficient of the product at the probe wavelength. For $n > 1$, eq 2 has the solution

$$I(z,r;t) = I(0,r,t)/(1 + \beta_n z(n-1)I(0,r,t)^{n-1})^{1/(n-1)} \tag{5}$$

Combining eqs 1−5, the transmission of the pump light T_p through the sample is given by

$$T_p = (2/\sqrt{\pi}J_p\rho_p^2\tau_p) \int_0^\infty dr\, r \int_{-\infty}^{+\infty} dt\, I(L,r;t) \tag{6}$$

and the photoinduced change ΔT_{pr} in the transmission T_{pr} of the probe light is given by

$$-\Delta T_{pr} =$$
$$\frac{2}{\rho_{pr}^2} \int_0^\infty dr\, r \exp\left(-\frac{r^2}{\rho_{pr}^2} - \frac{\phi_n\beta_e}{n}\int_{-\infty}^{+\infty} dt\, [I(0,r;t) - I(L,r;t)]\right) \tag{7}$$

where $I(L,r;t)$ is given by eq 5 for $z = L$ and ρ_{pr} is the $1/e$ radius of the Gaussian probe beam. The photoinduced change ΔOD in the decadic optical density of the sample (i.e., the TA signal) is related to the quantity given by eq 7 by $\Delta OD = -\log(1 + \Delta T_{pr}/T_{pr})$. Using eqs 6 and 7, the absorption coefficient β_n and the quantum yield ϕ_n can be determined for the known parameters ρ_p, τ_p, and ρ_{pr} from the dependencies of ΔOD and T_p vs J_p (Figure 1). For $\rho_{pr} \ll \rho_p$, only the beam of light with $r \approx 0$ can be considered, and the averaging over the polar coordinate in eq 7 is unnecessary. In such a case, the function $C(z) = c(z,r=0;t=+\infty)$ gives the concentration profile of the reaction product along the path of the probe light (Figure 2a).[17] The higher the pump irradiance, the steeper is this profile. By using these concentration profiles, the decay kinetics of the electron due to cross recombination in the bulk can be simulated (Figure 2b and section 3.4).

In Figure 1, a typical dependence of the TA signal from the electron for $\lambda = 800$ nm probe light (trace i) and 400 nm light transmittance of the pump laser pulse (trace ii) vs the incident pump irradiance is shown by symbols. The TA signal of the
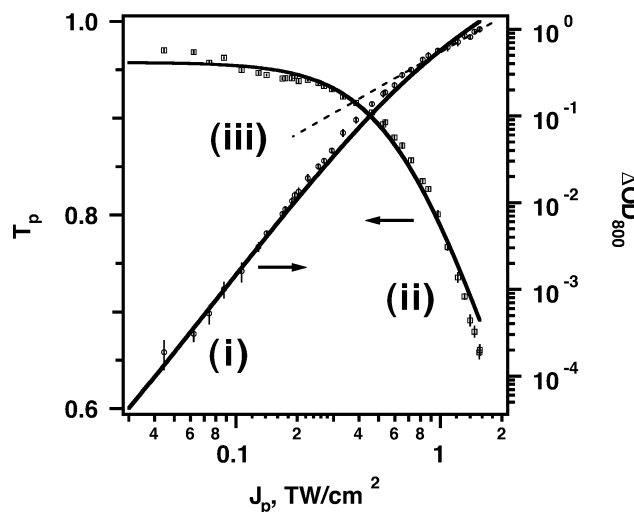
Figure 1. (i) Transmittance T_p of the 400 nm pump light (to the left, open squares), and (ii) TA signal ΔOD_{800} (obtained using $\lambda = 800$ nm, 60 fs fwhm probe light) from the photoelectron, e_{aq}^-, at the delay time of $t = 5$ ps (to the right, open circles) in three 400 nm photon laser excitations of the room temperature water flowing in a high-speed optical path $L = 70$ μm liquid jet. These two simultaneously determined quantities are plotted against the (peak) photon irradiance J_p of the incident 400 nm light. The vertical bars indicate 95% confidence limits. The beam parameters are $\rho_p = 126$ μm, $\tau_p = 120$ fs, and $\rho_{pr} = 24$ μm. Solid lines are quantities T_p and ΔOD_{800} simulated by using eqs 6 and 7 given in section 3.1, using the optimum fit parameters $\phi_3 = 0.415$ for the 3-photon quantum yield of photoionization and $\beta_3 = 267$ cm^3/TW^2 for the absorption coefficient of water; a molar absorptivity of 18 500 M^{-1} cm^{-1} for e_{aq}^- has been assumed. The dashed line (iii) drawn through the data points in the terawatt regime indicates the region where the electron absorbance increases linearly with the light irradiance (and the tentative "3+1" photoexcitation might have occurred).

(hydrated) electron along the path of 800 nm light traversing the $L = 70$ μm thick water jet was determined at the delay time of 5 ps, when the thermalization dynamics is over and the geminate recombination of the electron is still negligible (section 3.4). For this measurement, the pump pulse was 189 fs fwhm ($\tau_p = 120$ fs) and the $1/e$ radii of the pump and probe beams were $\rho_p = 126$ μm and $\rho_{pr} = 24$ μm (eq 1), respectively. The refractive index n_w of water of 1.343 for 405 nm light obtained in ref 20 was used to calculate the reflectivity of the jet surface, $R = 0.0214$ (multiple reflections were neglected), and the pump irradiance used in eq 1 was corrected by a factor of $(1 - R)$. The decadic molar absorptivity of 18 500 M^{-1} cm^{-1} for the hydrated electron was used.[16] The solid lines in Figure 1 are least-squares fits to eqs 6 and 7 assuming a 3-photon photoprocess ($n = 3$), which gave the optimum parameters $\beta_3 = 267$ $\pm$ 4 cm^3/TW^2 (i.e., 2.7×10^{-28} m^3/W^2) and $\phi_3 = 0.415 \pm 0.006$ (these error limits specify the standard deviation for a particular fit of the dependencies shown in Figure 1). The absorption coefficient β_3 obtained in this study is considerably lower than 900 cm^3/TW^2 given by Naskrecki et al.,[20] who used a thicker, 1 cm optical path sample and low-irradiance 400 nm light (<0.1 TW/cm^2) for water photoexcitation. Such disagreements are fairly typical for measurements of photophysical parameters for multiphoton excitation.[17a]

As seen from the linear section of the plot of ΔOD_{800} vs J_p given in Figure 1, the power law, $\Delta OD_{800} \propto J_p^3$, holds to $J_p < 0.3$ TW/cm^2. Above this irradiance, the TA curve bends down; in the same range, the transmission of 400 nm light rapidly decreases with increase in the irradiance. The bending over of the photoinduced absorption is due to the nonuniformity of the 400 nm light absorption by the jet; the typical (simulated) concentration profile $C(z)$ of the photoelectrons along the beam
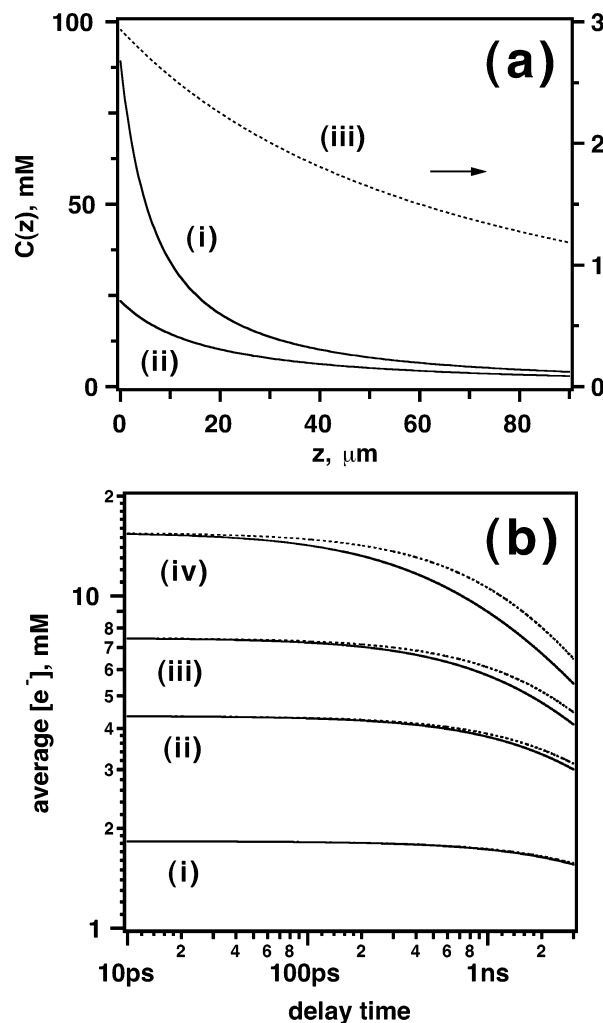

Figure 2. (a) Concentration profiles $C(z)$ of the photoelectrons generated by 400 nm laser pulse along the axis of the 400 nm beam. The electron concentrations, in units of 10^{-3} mol/dm^{-3} (mM), at the end of a radius 50 μm (eq 1), 330 fs fwhm, 400 nm pulse are plotted for three peak irradiances J_p of the 400 nm light: (i) 1.56, (ii) 1.0, and (iii) 0.5 TW/cm^2. (Trace iii is to the right, traces i and ii are to the left.) These concentration profiles are plotted against the penetration depth z of the 400 nm light for a 90 μm thick water jet. These traces were simulated by using the photophysical parameters given in the caption to Figure 1. The concentrations of the electrons at the jet surface (where $z = 0$) and the mean concentrations across the jet are respectively (i) 90 and 15.5 mM, (ii) 23.5 and 7.5 mM, and (iii) 2.9 and 1.8 mM. The higher the light irradiance, the shorter the effective path of the excitation light. (b) Evolution of the mean electron concentration for the same photosystem, assuming cross recombination in the water bulk with a bimolecular rate constant k_r of 3×10^{10} M^{-1} s^{-1} (assuming no geminate recombination). Traces i–iv correspond to pump irradiances of 0.2, 0.5, 1.0, and 1.56 TW/cm^2, respectively. The solid lines are obtained by averaging the decay kinetics $C(z,t)$ of the electron over the corresponding concentration profile: $\langle C(z,t)\rangle = \langle C(z)/(1 + ktC(z))\rangle$. The dashed lines correspond to a hypothetical system in which the electrons are generated homogeneously across the jet, with the initial concentration equal to the mean concentration obtained by averaging over the profiles given in part a, i.e., for $\langle C(z,t)\rangle = \langle C(z)\rangle/(1 + kt\langle C(z)\rangle)$. As the irradiance of 400 nm light increases, spatial inhomogeneity of the electron production has progressively greater effect on the electron decay by cross recombination.

axis for $J_p = 1.6$ TW/cm^2 is shown in Figure 2a, trace i. Compare this profile with the concentration profiles simulated for lower irradiance, $J_p = 1$ TW/cm^2 (Figure 2a, trace ii) and $J_p = 0.5$ TW/cm^2 (Figure 2a, trace iii). It is seen that in the terawatt regime, most of the 400 nm light is absorbed in a thin 10 μm layer near the jet surface. This shortening of the effective

Multiphoton Ionization of Liquid Water

J. Phys. Chem. A, Vol. 108, No. 42, 2004 **9109**

optical path of the probe light is the reason for slowing down (seen in Figure 1) of the increase in the ΔOD_{800} with increasing J_p. When a straight line is drawn on this double logarithmic plot through the data points for which $J_p > 0.5$ TW/cm² (trace iii in Figure 1), the slope of this line is close to unity, and this behavior initially led us to believe that "3+1" photoexcitation is vigorous in this terawatt regime. A detailed model for this "3+1" photoprocess is given in the Appendix and Figures 1S, 2S, and 3S in the Supporting Information. As seen from Figure 2S therein, the suggested absorption of 400 nm photons by photoproducts (e.g., electrons) is not needed to explain the power dependencies shown in Figure 1, insofar as the inhomogeneous light absorption alone explains the observed trend. Furthermore, as shown in the Appendix, when the occurrence of the "3+1" photoexcitation is postulated, the fit quality in Figure 1 does not improve.

While the general behavior shown in Figure 1 was reproducible, the power dependencies of the TA for $J_p > 1$ TW/cm² varied somewhat when the excitation conditions and beam geometries were changed between the runs (see several series of the TA measurements plotted together in Figure 4S). As shown below, in this terawatt regime, the heat release and thermal lensing by the photoexcited sample are significant and cause irreproducibility.

3.2. Thermalization Dynamics and the Electron Spectrum in the Terawatt Regime. As mentioned in the Introduction, one of the most striking kinetic transformations that occur in the terawatt regime is the change of short-term electron dynamics ($t < 10$ ps) occurring during the thermalization, relaxation, and hydration of the electron. The typical evolution of $\lambda = 1.2\ \mu$m kinetics as a function of pump irradiance is shown in Figure 3a (on a double logarithmic scale) and Figure 3b (on a linear scale, after normalization at $t = 5$ ps). As the pump irradiance increases from 0.4 to 2.1 TW/cm² the relative amplitude of the initial "spike" decreases almost 3 times. This "spike" is from a short-lived precursor of the hydrated electron whose absorption spectrum in the near-IR undergoes a rapid blue shift in the first 2 ps after photogeneration.[11–15,21] In Figure 4, the ratio of the $t = 10$ ps and the "spike" absorbance signals for $\lambda = 1.2\ \mu$m are plotted vs the 400 nm light irradiance. For the pump irradiance <1 TW/cm², the ratio of these two absorbance signals changes little as a function of the laser power. However, above 1 TW/cm², there is a rapid increase in the ratio with the laser power, indicating considerable flattening of the thermalization kinetics in the terawatt regime (which is also apparent from Figure 3b). The remarkable feature of Figure 4 is the abruptness of the transition between the low-irradiance and high-irradiance regimes.

The relative decrease in the amplitude of the "spike" with increasing pump power becomes lower at shorter wavelength of the probe light. For $\lambda = 1.05$ and $1.1\ \mu$m kinetics, the effect is smaller (Figure 5S); for $\lambda < 800$ nm, no change of the thermalization kinetics with the pump irradiance is observed (Figure 6S). While the thermalization stage is over in 5 ps, the electron spectra obtained in the terawatt regime ($J_p = 1.9$ TW/cm²) at $t = 50$ ps are still red-shifted with respect to the electron spectra of hydrated electrons in room temperature water (Figure 5a). As known from nanosecond pulse radiolysis studies,[16,22,23] the latter spectra undergo systematic red shift with increasing water temperature (see the Supporting Information for the explicit temperature dependencies of the spectral parameters). From these data, it is possible to estimate the solvent temperature corresponding to the red shift observed in Figure 5a. The surprising answer is that this temperature jump is very substan-
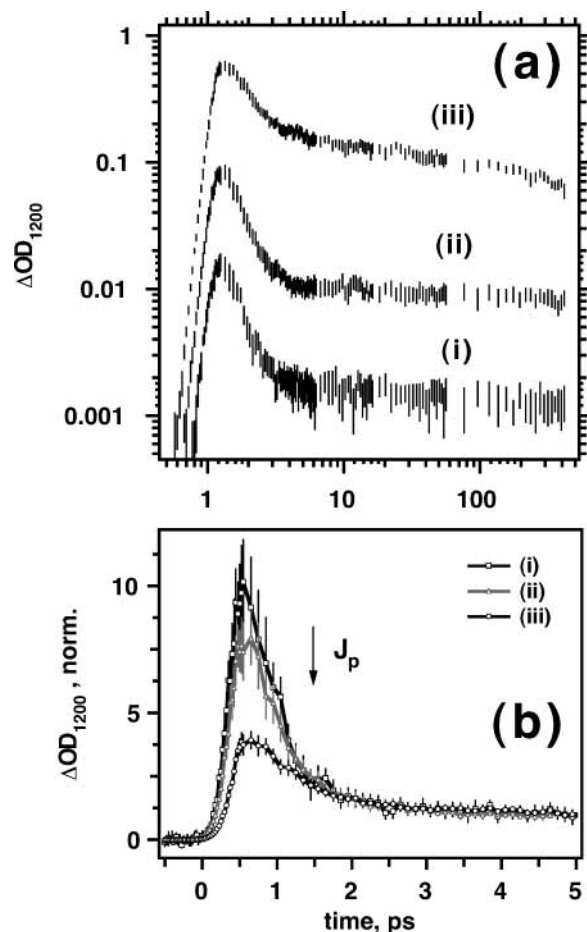

Figure 3. Pump−probe TA kinetics of photoelectrons (observed at $\lambda = 1.2\ \mu$m) generated in three 400 nm photon excitations of water (same beam geometry as that specified in Figure 2a). The 400 nm light irradiance J_p is (i) 0.4 (open squares), (ii) 1.23 (open triangles), and (iii) 2.1 TW/cm² (open circles). In part a, the kinetic traces are given on a double logarithmic plot. Note the relative decrease in the initial "spike" with increasing pump irradiance and the occurrence of second-order decay in trace iii. In part b, the kinetic traces normalized at $t = 5$ ps are shown. As the 400 nm irradiance increases, the ratio of the $t = 5$ ps signal to the maximum signal in the "spike" increases three times.

tial, since the position of the maximum of the absorption band corresponds to a bulk temperature of 80 °C. The origin of this temperature increase and the red shift of the "thermalized" spectrum (Figure 5b) is discussed in the next section. Below, we give a qualitative explanation of how the temperature jump accounts for the observed changes in the thermalization kinetics as observed by pump−probe TA spectroscopy:

When the localized, prethermalized electron is generated by photoionization of water, it has >1 eV excess energy and consequently its spectrum is not too sensitive to the temperature of the medium. From the standpoint of laser spectroscopy, the thermalization process can be viewed as a systematic blue shift of the absorption band of this electron in the visible and near-IR.[11–15,21] Unlike the spectrum of the initial, prethermalized species, the spectrum of the thermalized electron strongly depends on the water temperature, systematically shifting to the red with increasing temperature.[16,22,23] Thus, in hot water the blue shift of the electron band during the thermalization/hydration process becomes progressively smaller with increasing temperature. Since the "spike" in the TA kinetics observed to the red of 800 nm is due to this spectral shift, this "spike" (after normalization by the $t = 5$ ps absorbance) becomes relatively
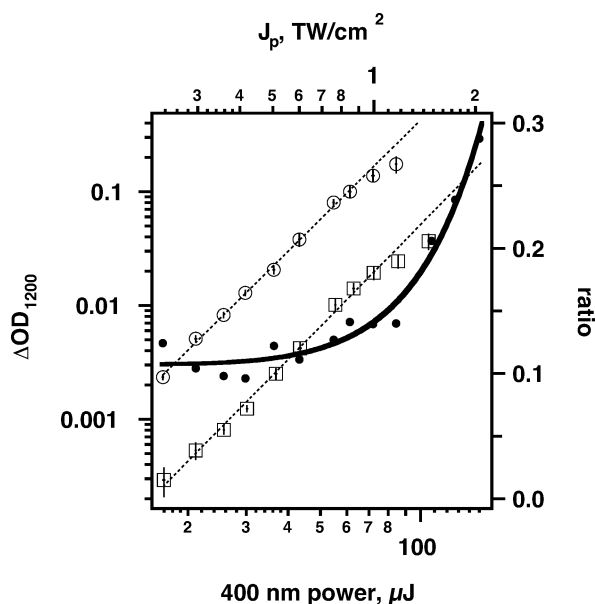
Figure 4. The irradiance dependencies of the TA signals ($\lambda = 1.2$ μm) for the photosystem shown in Figure 3. Open squares and open circles (to the left) indicate the TA signals from the photoelectron at $t = 5$ ps and at the "spike" maximum, respectively. (The points for $J_p >$ 1.5 TW/cm² are not shown.) The vertical bars give 95% confidence limits for these data points. The filled circles (to the right) give the ratio of these two absorbance signals. The smooth line drawn through these latter points is a guide for the eye. The dashed straight lines correspond to the power law increase in the TA signal amplitude; their slopes are close to 3.

smaller in amplitude as the temperature increases. This point is exemplified by Figure 6 in which thermalization dynamics of electrons observed at $\lambda = 1$ μm and normalized at $t = 5$ ps are given as a function of water temperature: 28, 57, and 85 °C (for 3-photon ionization of water with 0.2 TW/cm² 400 nm light). Similar changes in the near-IR kinetics as a function of water temperature have been observed by Unterreiner and co-workers.[14] These changes look remarkably similar to those observed for room temperature water in the terawatt regime. The fact that the time profiles of thermalization kinetics observed for $\lambda < 800$ nm (Figure 6S) do not change with the laser power does not contradict this picture: First, these kinetics change little in hot water (see ref 14). Second, our recent studies of electron thermalization in 200 nm biphotonic ionization of water suggest that the time profile of the kinetics observed at $\lambda = 450-700$ nm changes little with the wavelength λ.[21] Due to this weak dependence of the time profile on the water temperature and the wavelength, a red shift of a few tens of nanometers is inconsequential.

3.3. The Temperature Jump. In this section, the origin of the temperature jump observed in the terawatt regime is discussed. We emphasize that this temperature jump is not related to the "local" increase in temperature during electron thermalization. The latter has been postulated by Madsen et al.[24] and Keiding et al.[25] to account for subpicosecond relaxation of the electron, by rapid heat transfer to its surroundings. As seen from the previous section, in the terawatt regime, the water stays hot well after this relaxation stage is completed and the electron is in thermal equilibrium with its environment. In other words, the temperature jump observed in this regime is a bulk, macroscopic effect.

We suggest that the temperature jump is a natural consequence of the photophysics of 400 nm ionization. To demonstrate this point, we consider a particular set of excitation
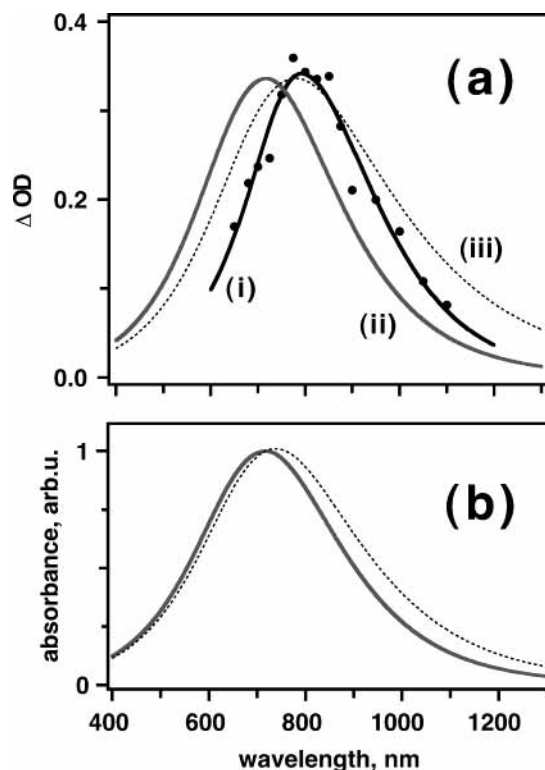

Figure 5. (a) Trace i gives the experimental TA spectrum of the photoelectron observed 50 ps after three 400 nm photon excitations of water in a 90 μm thick jet ($\rho_p = 73$ μm, $\rho_{pr} = 22$ μm, $\tau_p = 176$ fs) at a pump irradiance of 1.9 TW/cm². This spectrum was obtained by selecting probe pulses from the white light supercontinuum, using narrowband interference filters; focusing of these different light components at the sample varied slightly across the absorption spectrum. For the multiphoton ionization, the TA signal is very sensitive to the pump and probe beam overlap, and the amplitude of the points close to 800 nm (for which the probe beam was more focused) is somewhat greater than that in the wings of the TA spectrum. Even with this (hard to avoid) distortion of the TA spectrum in mind, it is apparent that the spectrum is red-shifted relative to the absorption spectrum of thermalized electron in room temperature water (trace ii). Trace iii corresponds to the spectrum of thermalized electron in 80 °C water. (b) The solid line is trace ii reproduced from the plot above; the dashed line is the average spectrum of (thermalized) electrons that was obtained with use of the concentration profile trace i shown in Figure 2a and the e_{aq}^- spectrum parametrization given in the Supporting Information (see section 3.3 for more detail).

conditions given in the caption to Figure 2. In Figure 2a, trace i, the concentration profile of electrons simulated by using ϕ_3 and β_3 obtained in section 3.1 is plotted vs the penetration depth z of 400 nm, $J_p = 1.6$ TW/cm² light. At the surface of the jet, the electron concentration is ca. 90 mM, while the concentration averaged over the 90 μm thick jet is ca. 6 times lower. The deposition of the light energy into water follows the same profile, i.e., the concentration of electrons is maximum exactly where most energy is deposited. If all of this absorbed energy were used to ionize the solvent, relatively little heat from the electron thermalization would be deposited into water (which would account, by a conservative estimate, for the release of 1 eV of heat per ionization event). However, as shown in section 3.1, the quantum yield ϕ_3 of 3-photon ionization is only 0.42. Assuming that water molecules that do not ionize dump the excess energy into the bath, we obtain that 5.5–6.5 eV of the total absorbed energy (equal to 9.3 eV) ends up as heat (the exact estimate depends on how the energy released in the electron thermalization and H–OH dissociation is counted). At the surface, the density of the energy absorbed by water is ca.
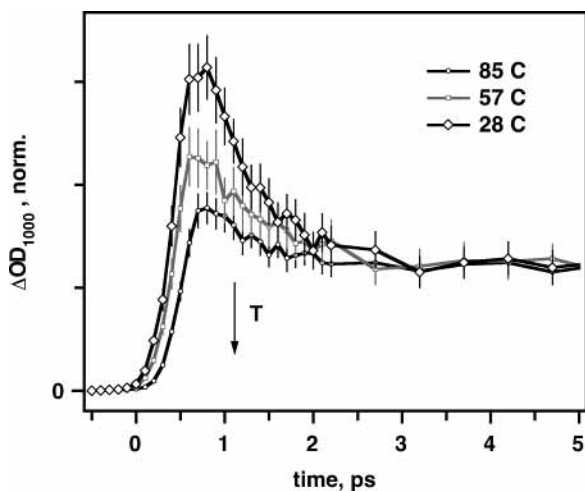
Figure 6. Thermalization kinetics of the electron observed with use of pump−probe TA spectroscopy ($\lambda = 1\ \mu$m) for three 400 nm photon excitations of water at 28 (open diamonds), 57 (open squares), and 85 °C (open circles). The peak irradiance J_p of the 400 nm light was fairly low, $J_p = 0.2$ TW/cm^2, so that the light-induced temperature jump was negligible. To facilitate the comparison of the time profiles, these TA kinetics are normalized at $t = 5$ ps, at which delay time the thermalization stage is complete. As the water temperature increases, the relative amplitude of the "spike" decreases.

190 J/cm^3, which is equivalent to 46 cal/g. The heat capacity C_w of water is 1 cal g^{-1} K^{-1} and the density ρ_w is 1 g/cm^3.[26] Provided that 60% of the absorbed energy is released as heat, the temperature of water would increase by 28 °C. By using the spectroscopic data of Bartels and co-workers,[22] it can be shown that to double the 1.1 μm absorbance of the hydrated electron by a temperature-induced red shift of its absorption spectrum, a thermal jump of 33 °C would be sufficient. The temperature jump rapidly decreases as a function of the penetration depth of the 400 nm light. However, since the electron concentration tracks the same profile, the resulting spectral shift is still substantial. By using the parametrization of the e_{aq}^- spectrum as a function of temperature given by Bartels and co-workers[22] and averaging along the path of the beam, a sample-average spectrum in Figure 5b was obtained. This spectrum is notably red shifted with respect to the equilibrium e_{aq}^- spectrum at 25 °C.

Importantly, once the heat is released, the equilibration of the solvent across the jet would take a long time. The heat conductivity κ_w of water is 6 mW cm^{-1} K^{-1} so that the heat diffusivity $\mu_w = \kappa_w/\rho_w C_w$ is 1.4×10^{-3} cm^2/s.[26] A temperature gradient over 10 μm (the same as the concentration gradient shown in Figure 2a) would take ca. 0.3 ms to disappear by diffusive heat exchange. Thus, the temperature stays constant on the subnanosecond time scale of our kinetic observations. Another important point is that homogenization of the heat on the microscopic scale would be rapid. In the model discussed above, the heat release and water ionization occur in different excitation events, i.e., to observe the effect of the heat (the temperature jump) on the electron spectrum and geminate recombination and thermalization dynamics, the heat released in an excitation event should reach the environment of the electron generated in a separate ionization event. It is the latter consideration that explains why the kinetic transformations observed in the terawatt regime are relatively abrupt: not only should a sufficient amount of heat be released to generate the temperature jump, the density of the excitation events should be sufficiently high as well, otherwise, the heat release in spatially isolated events would have little effect on the short-

term dynamics. Again, the photophysics of three 400 nm photon excitations are such that the critical density of these events is achieved in the same regime where the temperature jump is substantial. For example, the electron concentration at the surface of the jet in Figure 2a, trace i, is so high that the average distance between the excitation events is ca. 1.6 nm; on this scale, thermal equilibration of the solvent would take only 3 ps.

In the estimates for the instantaneous temperature jump given above, H−OH bond dissociation of photoexcited water molecules was neglected. The branching ratio between water ionization and bond dissociation in three 400 nm photon excitations of water is not known. In two 266 nm photonic excitations of water, Thomsen et al.[25] estimated that the branching ratio between the dissociation and ionization is 0.55:1. Note that rapid recombination of caged H and OH radicals deposits the heat back into the solvent.

3.4. Geminate Kinetics and the Escape Probability. Since the amplitude of the TA signal from the electron changes very rapidly with 400 nm light irradiance, it is difficult to obtain good quality kinetics in the low and high power regimes by using the same sample. At low power, the absorption is weak and a relatively thick sample is needed to obtain a TA signal of $(1-10) \times 10^{-3}$ OD to sample the geminate kinetics with a reasonable signal-to-noise ratio. Conversely, at intermediate and high pump power, only short-path high-speed jets could be used to avoid damage to the sample.

In the terawatt regime, the yield of the electrons is so high that cross recombination in the bulk solvent begins to occur on the subnanosecond time scale. This effect is mainly the consequence of inhomogeneous absorption of light.[9,17] In Figure 2b (solid lines), the decay kinetics for homogeneous recombination of electrons averaged along the path of the probe light are simulated for the initial concentration profiles shown in Figure 2a, as a function of the pump irradiance, assuming a (bulk) recombination constant of 3×10^{10} M^{-1} s^{-1} (close to the rate constant of $e_{aq}^- + OH_{aq}$ recombination at 25 °C). A slightly greater rate constant of 3.8×10^{10} M^{-1} s^{-1} for cross recombination of e_{aq}^- in water ionized by the intense 266 nm laser was obtained by Pommeret et al.[17b] For comparison, dashed lines in Figure 2b give the recombination kinetics obtained assuming homogeneous generation of the electrons along the path of 400 nm light (the initial concentration had the same value as the mean concentration for the corresponding $C(z)$ profile shown in Figure 2a). It is seen that the recombination kinetics are much faster for the inhomogeneous distribution, in agreement with the experimental results discussed below. Thus, at the higher end of the pump irradiance, the kinetic profiles observed within the first 600 ps after the ionization are strongly affected by the cross recombination; the latter cannot be fully disentangled from the geminate recombination which occurs on the same time scale.

Figure 7, trace i, shows typical pump−probe kinetics for 800 nm absorbance from water excited by 400 nm light (0.1 TW/cm^2) obtained by using a 5 mm optical path flow cell ("normal" beam geometry with $\rho_p = 92\ \mu$m and $\rho_{pr} = 12.2\ \mu$m). The initial "spike", which has the same time profile as the response function of our setup, is due to nonlinear absorbance (simultaneous absorbance of 400 and 800 nm photons). As the pump irradiance increases and more 400 nm light is absorbed by the sample, fewer 400 nm photons are available for this nonlinear process, and the relative amplitude of the "spike" decreases dramatically. The slow decay on time scales of 10 to 600 ps is due to the geminate recombination of hydrated electrons; heat release and cross recombination are negligible in this low-power regime.
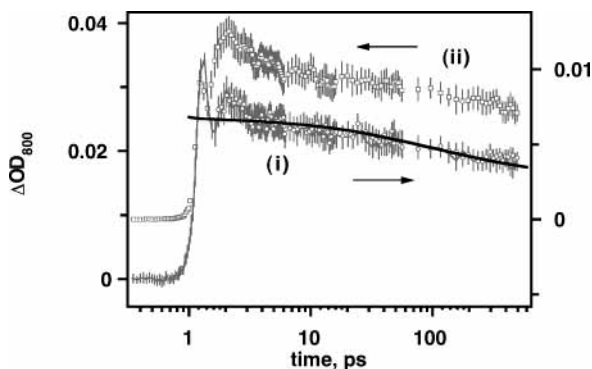
Figure 7. Pump−probe TA kinetics of the electron generated by three 400 nm photon excitations of water in (i) a 5 mm optical path cell (J_p = 0.125 TW/cm^2; open circles, to the right) and (ii) a 560 μm thick liquid jet (J_p = 0.2 TW/cm^2; open squares, to the left). The solid curve is the simulation of the geminate recombination dynamics with use of the IRT model given by Pimblott and co-workers, ref 36 (the model parameters are given in the caption to Figure 1S in the Supporting Information; see also ref 2) for an initial r^2-Gaussian electron distribution, eq A1, with a width parameter σ_0 = 1.1 nm.
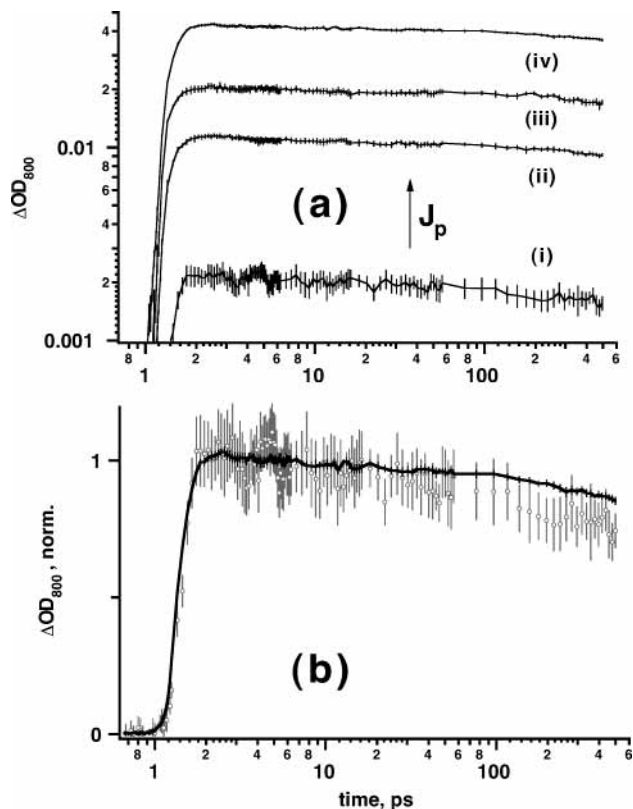

Figure 8. (a) The evolution of the TA kinetics of the electron (λ = 800 nm, ρ_p = 83 μm, τ_p = 200 fs, ρ_{pr} = 232 μm) generated by 400 nm photoionization of water in a 90 μm thick jet as a function of the pump irradiance for J_p = (i) 0.29, (ii) 0.65, (iii) 1.3, and (iv) 2.6 TW/cm^2. Note that the "reverse" beam geometry was used for these kinetic measurements. (b) A comparison between the time profiles of normalized kinetic traces i (open circles) and iv (solid line) from Figure 8a.

Very similar kinetics (save for the smaller amplitude of the "spike") were obtained for 0.2 TW/cm^2 excitation of water in a 560 μm thick high-speed liquid jet (see trace ii in Figure 7; ρ_p = 85 μm and ρ_{pr} = 10 μm).

Parts a and b of Figure 8 show TA kinetic traces (λ = 800 nm) obtained at higher pump irradiances. Figure 9 shows the TA signals at t = 500 and 10 ps plotted as a function of J_p (these data were obtained by using the "reverse" beam geometry: ρ_p = 85 mm and ρ_{pr} = 190 mm). The ratio of these two
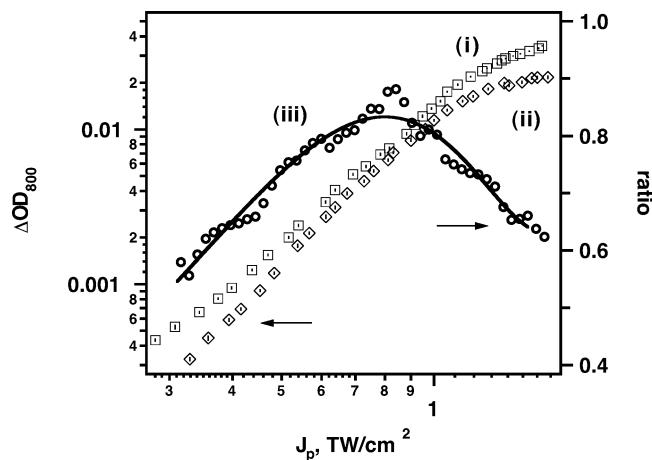

Figure 9. Pump irradiance dependencies of the TA signals at (i) t = 10 (open squares; to the left) and (ii) 500 ps (open diamonds; to the left) in three 400 nm photoexcitations of water in a 90 μm thick jet (λ = 800 nm, ρ_p = 85.4 μm, τ_p = 200 fs, ρ_{pr} = 190 μm; note that "reverse" beam geometry was used). Trace iii (open circles; to the right) is the ratio of the t = 500 10 ps absorbance signals. The solid line is a guide to the eye.

TA signals plotted in the same figure is a measure of the fraction of electrons that escape recombination at t = 500 ps. As seen from Figure 9, for J_p > 0.3 TW/cm^2 this ratio first increases with the pump irradiance; then, at around 1 TW/cm^2, it begins to decrease. The latter changeover occurs in the same range where rapid cross recombination is expected to occur, and the kinetics shown in Figure 8 (see also Figure 3a, trace iii, and Figure 7S) reveal the long-term effects of such a recombination, which are similar to those simulated in Figure 2b. (Note that for the TA kinetics obtained by using the "reverse" beam geometry, cross recombination is less prominent since the average concentration of electrons across the pump beam,which is probed by using this geometry, is substantially lower than that at r = 0, which is probed by using the "normal" beam geometry.) Even those TA kinetics that are affected by the homogeneous recombination on a subnanosecond time scale show the same short-term behavior as the kinetics obtained in the 0.3−1 TW/cm^2 range (Figures 8b and 7S). In particular, within the first 100 ps after the 400 nm photoexcitation, these kinetics are much flatter than the kinetics shown in Figure 7. To some degree, this flattening of the kinetic traces is due to the changes in the thermalization dynamics. The latter can be eliminated by comparing TA kinetics normalized at t = 10 ps, when the (power-dependent) electron thermalization is complete. The geminate electron decay certainly slows down (Figures 8 and 7S) and the survival probability increases (Figure 9) with increasing irradiance of the 400 nm light. Most of this change occurs in a narrow range of pump irradiance, between 0.5 and 1 TW/cm^2. At higher irradiance, this trend is difficult to follow because the cross recombination interferes with the geminate recombination. Importantly, the range in which the geminate kinetics change with increasing J_p is the same range in which the thermalization kinetics also begin to change. The latter kinetics are, actually, less sensitive to the photogenerated release of heat because a high critical concentration of the excitation events (achieved only for J_p > 1 TW/cm^2) is needed for rapid homogenization of the heat on the picosecond time scale, as noted in section 3.2.

We believe that the geminate recombination kinetics observed in the terawatt regime are for the hydrated electron in *hot* water and explain the observed transformations by the temperature jump:

Multiphoton Ionization of Liquid Water

J. Phys. Chem. A, Vol. 108, No. 42, 2004 **9113**

The effect of increasing temperature on the geminate recombination in water has been studied by Madsen et al.[24] (who followed the electron decay kinetics to $t = 90$ ps). The main effect is to increase the survival probability of the electron, from ca. 0.55 at 10 °C to 0.75 at 80 °C (at $t = 90$ ps, see Figure 4 in ref 24). Interestingly, while diffusion is faster in hot water, the geminate recombination after the first 10 ps becomes slower. Madsen et al. explain these observations by the decrease in the dielectric constant of water and the fact that recombination of the electron, e_{aq}^-, with the OH radical is not diffusion controlled at the higher temperature, so that the probability that a diffusion encounter leads to recombination of the (OH, e_{aq}^-) pair decreases. Such pairs, by the estimate of Madsen et al.,[24] account for 80% of all recombination events after water photoionization; the remaining 20% are from the recombination of e_{aq}^- with the hydronium ion, H_3O^+. Recently, Crowell et al.[18] studied the temperature effect on the dynamics of (OH, e_{aq}^-) pairs generated by 200 nm light induced electron photodetachment from aqueous hydroxide. The decay kinetics of the electron were followed out to 600 ps, and the temperature range of 8 to 90 °C was explored (see Figures 3 and 4 in ref 18a). The changes of the long-term kinetics with increasing temperature observed for this closely related photosystem are remarkably similar to those observed by Madsen et al. in water:[24] the electron escape becomes more efficient and the diffusional "tail" of the kinetics becomes flatter. These trends are also present in the kinetics observed in the terawatt regime for 400 nm photoionization of neat water. While we do not have sufficient data to demonstrate by rigorous simulation that the heat release alone causes *all* of the observed kinetic transformations,[27] the qualitative behavior is consistent with the notion that the changes in the geminate kinetics are of the same origin as the concurrent changes in the thermalization dynamics.

3.5. Implications for Pulse Radiolysis of Water. In pulse radiolysis of condensed-matter systems, the excitation energy of the ionizing particle is deposited very unevenly: the excitation/ionization events are clustered in a small volume of $2-5$ nm diameter (the so-called radiolytic spur); these spurs are separated by vast distances (ca. 100 nm along the particle track).[28] It has been speculated by Eisenthal and co-workers[29] and others[30] that rapid heat deposition in spurs could change the kinetics observed on the picosecond time scale, before the heat dumped into the media during electron thermalization escapes from the spur. Until recently, there was little support for such an assertion. However, recent observations from two laboratories[31,32] seem to provide such support. It appears that the temperature jump observed in multiphoton ionization of water (see above) also occurs in water radiolysis, though the dynamics of the two effects are quite different.

Recently, Gauduel et al.[31] studied the electron dynamics in room temperature liquid H_2O using a novel technique of femtosecond pump–probe pulse radiolysis–TA spectroscopy. The 700 fs fwhm pulse of relativistic $(2-15$ MeV) electrons was generated by interaction of a 10 TW amplified Ti:sapphire laser pulse with a supersonic helium jet.[33] The TA signal from hydrated electron was observed at 820 nm and followed over the first 150 ps after the radiation-induced water ionization. These kinetics were qualitatively different from the ones extrapolated from the pump–probe data obtained on a longer time scale, in both pulse radiolysis[34] and multiphoton excitation.[1,2,3,9,21,24,25] Specifically, instead of smooth, sloping decay curves similar to those shown in Figure 8, a fast component with an exponential lifetime of ca. 20 ps was observed. Since the kinetics observed for $t > 50$ ps[29,32,34] are indicative of a

broad initial distribution of electron–hole distances, the 20 ps component could not be accounted for by the geminate recombination. On the other hand, the relatively long lifetime of this component (as compared to the characteristic time of the solvation dynamics, <300 fs)[12-14] excludes the involvement of presolvated electron. The same 20 ps component, albeit smaller in amplitude, was observed by Wishart et al.[32] at the probe wavelength of 1000 nm using the picosecond laser cathode driven linac facility (LEAF)[35] at the Brookhaven National Laboratory (Figure 8Sa).

This short-term behavior might be qualitatively accounted for by a temperature jump in the radiolytic spur.[29,30] The difference between the photolysis and radiolysis is that for the latter, heating of water is localized on the nanoscale.

In the near-IR, the molar absorptivity of the electron plotted vs the local temperature passes through a maximum at >100 °C (Figure 8Sb). When the local temperature in the spur decreases on the picosecond time scale, this causes the *decrease* in the TA in this spectral region. Assuming that the distribution of the local temperatures follows that of the electrons (since the heat is deposited during the electron thermalization), the characteristic cooling time of a spur of the size a is a^2/μ_w.[30] For $a = 2$ nm, an estimate of $20-30$ ps is obtained—in reasonable agreement with the observed time constant for the fast component.[31,32] The substantial temperature jump is reasonable since the average energy required to ionize water by $2-15$ MeV electrons $(20-25$ eV)[28] is more than twice the optical gap of this liquid $(10-11$ eV).[3,4] This excess energy is released as heat during the electron thermalization, and the local temperature immediately after the electron hydration increases substantially. Simple estimates suggest a temperature jump of at least $30-40$ °C at the center of the spur.[29] As seen from trace ii in Figure 8Sb, such a temperature jump would be sufficient to account for the fast component observed at 1000 nm in the experiments of Wishart et al.[32] A simple way to verify this explanation would be to observe the electron dynamics at other probe wavelengths.

4. Conclusion

It is suggested that previously observed transformations of geminate recombination and electron thermalization kinetics in multiphoton ionization of liquid water by 400 nm terawatt light are caused mainly by rapid heat deposition into the bulk sample. The release of heat during the photoexcitation causes a nearly instantaneous temperature jump of several tens of degrees Centigrade. The ultimate cause of this jump is the low quantum yield for the 3-photon ionization of water: only 42% of the excitation events result in solvent ionization; the rest of the energy absorbed by water is released as heat. Consequently, the electron spectrum shifts to the red, the thermalization dynamics of the electron observed by TA in the near-IR become flatter, the geminate recombination dynamics become slower, and the survival probability (i.e., the escape fraction) of the electrons increases.

Our analyses suggest that the ionization of water by 400 nm light remains three photons up to the irradiance at which the water begins to break down; there is little evidence for the occurrence of "3+1" photoionization in which the electron or an excited water molecule generated during the ionization/excitation process absorbs one or more 400 nm photons. Though our experiments do not exclude such a possibility entirely, this photoprocess seems to be of little importance for the excitation of water by femtosecond pulses. Furthermore, it appears that the results can be understood, albeit qualitatively, without such a postulate, by water heating alone. It is likely that other reported

instances of power-dependent kinetics for hydrated electron generated by water ionization in the terawatt regime can be explained in the same way. It is also possible that the fast (ca. 20 ps) component that was recently observed in the ultrafast pulse radiolysis, transient absorption studies by Gauduel et al.[31] and Wishart et al.,[32] can be accounted for by a temperature jump in the radiolytic spur, as suggested almost 40 years ago by Ingalls et al.[30]

Supporting Information Available: Modeling of the photophysics for "3+1" excitation, equilibrium spectra of hydrated electron vs the solvent temperature, and Figures 1S−8S showing a detailed model for the 3+1 photoprocess and pump-probe TA kinetics plots. This material is available free of charge via the Internet at http://pubs.acs.org.

References and Notes

(1) Crowell, R. A.; Bartels, D. M. *J. Phys. Chem.* **1996**, *100*, 17940 and references therein. Bartels, D. M.; Crowell, R. A. *J. Phys. Chem. A* **2000**, *104*, 3349.

(2) Crowell, R. A.; Bartels, D. M. *J. Phys. Chem.* **1996**, *100*, 17713.

(3) Sander, M. U.; Gudiksen, M. S.; Luther, K.; Troe, J. *Chem. Phys.* **2000**, *258*, 257 and references therein. Sander, M. U.; Luther, K.; Troe, J. *J. Phys. Chem.* **1993**, *97*, 11489.

(4) Bernas, A.; Ferradini, C.; Jay-Gerin, J.-P. *Chem. Phys.* **1997**, *222*, 151. Houee-Levin, C.; Tannous, C.; Jay-Gerin, J.-P. *J. Phys. Chem.* **1989**, *93*, 7074.

(5) Hilcer, M.; Bartczak, W. M.; Sopek, M. *J. Chem. Phys.* **1986**, *85*, 6813. Hilczer, M.; Bartzak, W. M.; Kroh, J. *J. Chem. Phys.* **1988**, *89*, 2286. Bartzak, W. M.; Sopek, M.; Kroh, J. *Radiat. Phys. Chem.* **1989**, *34*, 93. Hilcer, M.; Bartzak, W. M. *Radiat. Phys. Chem.* **1992**, *39*, 85. Bartzak, W. M.; Pernal, K. *Res. Chem. Intermed.* **2001**, *27*, 891.

(6) Mozumder, A. *Radiat. Phys. Chem.* **1988**, *32*, 287. Tachia, M.; Mozumder, A. *J. Chem. Phys.* **1974**, *60*, 3037.

(7) McGowen, J. L.; Ajo, H. M.; Zhang, J. Z.; Schwartz, B. J. *Chem. Phys. Lett.* **1994**, *231*, 504.

(8) Long, F. H.; Lu, H.; Shi, X.; Eisenthal, K. B. *Chem. Phys. Lett.* **1991**, *185*, 47.

(9) Pommeret, S. In preparation.

(10) Son, D. H.; Kambhampati, P.; Kee, T. W.; Barbara, P. F. *Chem. Phys. Lett.* **2001**, *342*, 571. Son, D. H.; Kambhampati, P.; Kee, T. W.; Barbara, P. F. *J. Phys. Chem. A* **2001**, *105*, 8269. Son, D. H.; Kambhampati, P.; Kee, T. W.; Barbara, P. F. *J. Phys. Chem. A* **2002**, *106*, 2374.

(11) Pepin, C.; Goulet, T.; Houde, D.; Jay-Gerin, J.-P. *J. Phys. Chem. A* **1997**, *101*, 4351. Jay-Gerin, J.-P. *Can. J. Chem.* **1997**, *75*, 1310.

(12) Gauduel, Y. In *Ultrafast Dynamics of Chemical Systems*; Simon, J. D., Ed.; Kluwer: Amsterdam, The Netherlands, 1994; pp 81−136.

(13) Vilchiz, V. H.; Kloepfer, J. A.; Germaine, A. C.; Lenchenkov, V. A.; Bradforth, S. E. *J. Phys. Chem. A* **2001**, *105*, 1711.

(14) Hertwig, A.; Hippler, H.; Unterreiner, A. N.; Vohringer, P. *Ber. Bunsen-Ges. Phys. Chem.* **1998**, *102*, 805. Hertwig, A.; Hippler, H.; Unterreiner, A. N.; Vohringer, P. *Phys. Chem. Chem. Phys.* **1999**, *1*, 5663. Hertwig, A.; Hippler, H.; Unterreiner, A. N.; Vohringer, P. *J. Phys. Condens. Matter* **2000**, *12*, A165. Hertwig, A.; Hippler, H.; Unterreiner, A. N.; Vohringer, P. *Phys. Chem. Chem. Phys.* **2002**, *4*, 4412.

(15) Keszei, E.; Murphrey, T. H.; Rossky, P. J. *J. Phys. Chem.* **1995**, *99*, 22.

(16) Elliot, A. J.; Ouellette, D. C.; Stuart, C. R. *The Temperature Dependence of the Rate Constants and Yields for the Simulation of the Radiolysis of Heavy Water*; AECL report 11658; AECL Research: Chalk River Laboratories, Chalk River, Ontario, Canada, 1996. Jou, F.-Y.; Freeman, G. R. *Can. J. Chem.* **1979**, *57*, 591.

(17) (a) Pommeret, S.; Gobert, F.; Mostafavi, M.; Lampre, I.; Mialocq, J.-C. *J. Phys. Chem. A* **2001**, *105*, 11400. (b) Pommeret, S.; Gobert, F.; Mostafavi, M.; Lampre, I.; Mialocq, J.-C. *Res. Chem. Intermed.* **2001**, *27*, 901.

(18) (a) Lian, R.; Crowell, R. A.; Shkrob, I. A.; Bartels, D. M.; Chen, X.; Bradforth, S. E. *J. Chem. Phys.* **2004**, *120*, 11712. Crowell, R. A.; Lian, R.; Sauer, M. C., Jr.; Oulianov, D. A.; Shkrob, I. A. *Chem. Phys. Lett.* **2004**, *383*, 481. (b) See, for example: Schaffer, C. B.; Nishimura, N.; Glezer, E. N.; Kim, A. M.-T.; Mazur, E. *Opt. Express* **2002**, *10*, 196.

(19) Shkrob, I. A.; Crowell, R. A. *Phys. Rev. B* **1998**, *57*, 12207. von Behren, J.; Kostoulas, Y.; Burak Ucer, K.; Fauchet, P. M. *J. Non-Cryst. Solids* **1996**, *198−200*, 957. Fauchet, P. M.; Hulin, D.; Vanderhaghen, R.; Mourchid, A.; Nighan, W. L., Jr. *J. Non-Cryst. Solids* **1992**, *141*, 76.

(20) Naskrecki, R.; Menard, M.; van der Meulen, P.; Vigneron, G.; Pommeret, S. *Opt. Commun.* **1998**, *153*, 32.

(21) Lian, R.; Crowell, R. A.; Shkrob, I. A. *J. Phys. Chem. A.* To be submitted for publication.

(22) Bartels, D. M.; Takahashi, K.; Marin, T.; Jonah, C. D. *J. Phys. Chem. A.* In preparation; to be submitted for publication.

(23) Hart, E. J.; Anbar, M. *The Hydrated Electron*; Wiley-Interscience: New York, 1970; p 39.

(24) Madsen, D.; Thomsen, C. L.; Thogersen, J.; Keiding, S. R. *J. Chem. Phys.* **2000**, *113*, 1126.

(25) Thomsen, C. L.; Madsen, D.; Keiding, S. R.; Thogersen, J.; Christiansen, O. *J. Chem. Phys.* **1999**, *110*, 3453.

(26) *Handbook of Chemistry and Physics*, 69th ed.; Weast, R. C., Astle, M. J., Beyer, W. H., Eds.; CRC Press: Boca Raton, FL, 1988.

(27) For such an analysis, one needs to average over the geminate recombination kinetics in each layer of the jet, as the temperature decreases with the penetration depth of the 400-nm light. Presently, the temperature dependence of such kinetics on the subnanosecond time scale (in 3×400 nm photoionization of water) is lacking: these kinetics can be obtained in the low-power regime only, and the S/N ratio is too poor to track subtle changes in the TA signal. At higher irradiance, where the S/N ratio is more acceptable, it is impossible to discount the light-induced temperature jump.

(28) Pimblott, S. M.; Mozumder, A. In *Charged Particle and Photon Interactions with Matter*; Marcel Dekker: New York, 2004; p 75.

(29) Wang, Y.; Crawford; McAuliffe, M. J.; Eisenthal, K. B. *Chem. Phys. Lett.* **1980**, *74*, 160.

(30) (a) Mozumder, A. In *Advances in Radiation Chemistry*; Burton, M., Magee, J. L., Eds.; Wiley-Interscience: New York, 1969; Vol. 1. (b) Ingalls, R. B.; Spiegler, P.; Norman, A. *J. Chem. Phys.* **1964**, *41*, 837. Ingalls, R. B. *J. Chem. Phys.* **1966**, *44*, 1307. Burns, W. G.; Barker, R. In *Aspects of Hydrocarbon Radiolysis*; Gaumann, T., Hoigne, J., Eds.; Academic Press: New York, 1968; Chapter 2, pp 47−51.

(31) Gauduel, Y. et al. In preparation.

(32) Wishart, J. R.; Funston, A.; Cook, A. R. *Rev. Sci. Instrum.* Submitted for publication.

(33) Malka, V.; Fritzler, S.; Lefebvre, E.; Krushelnick, K.; Mangles, S. P. D.; Najmudin, J.; Walton, B.; Dangor, A. E. *Phys. Scr.* **2004**, *T107*, 141 and references therein.

(34) Pimblott, S. M.; LaVerne, J. A.; Bartels, D. M.; Jonah, C. D. *J. Phys. Chem.* **1996**, *100*, 9412 and references therein.

(35) Takeda, N.; Poliakov, P.; Cook, A. R.; Miller, J. R. *J. Am. Chem. Soc.* **2004**, *126*, 4301.

(36) Pimblott, S. M. *J. Phys. Chem.* **1991**, *95*, 6946.